SEMARAK ILMU PUBLISHING

Journal of Advanced Research in Applied Mechanics

Journal homepage:
https://semarakilmu.com.my/journals/index.php/appl_mech/index
ISSN: 2289-7895

Predicting Embedded Crack Growth Behaviour using S-version Finite Element Method of AlSi10Mg Material

Tan Sze Pei[1], Stephanie George Kana[1], Mohd Shamil Shaari[1,*], Akiyuki Takahashi[2], Mohd Akramin Mohd Romlay[1]

[1] Faculty of Mechanical and Automotive Engineering Technology, Universiti Malaysia Pahang, 26600 Pekan, Pahang, Malaysia
[2] Department of Mechanical Engineering, Faculty of Science & Technology, Tokyo University of Science, 2641 Yamazaki, Noda-shi, Chiba-ken 278-8510, Japan

ARTICLE INFO

Article history:
Received 25 October 2024
Received in revised form 26 November 2024
Accepted 3 December 2024
Available online 30 December 2024

Keywords:
Embedded crack; metallic additive manufacturing; AlSi10Mg; computational fracture mechanics

ABSTRACT

Cracks in materials may propagate at random behaviour and speed, eventually leading to catastrophic failure. For the characteristic of an embedded crack can be predicted using fracture mechanics. In this research, we employed an S-version finite element method (S-version FEM) to model and predict the crack growth behaviour of AlSi10Mg material produced using the powder-bed laser-fused method. The S-version FEM utilizes the mesh superimposed technique with a global-local mesh applied to the model. The simulation results computed the crack behaviour based on Paris' law approach, considering the stress intensity factor (SIF). Subsequently, the SIF results were evaluated using the virtual crack closure method (VCCM). A three-dimensional embedded crack was modelled within the local mesh. In order to anticipate how AlSi10Mg behaves when it undergoes crack propagation, the S-version FEM analysis was simulated for three different aspect ratios upon to the initial crack sizes. Then, the SIF results compared to an analytical solution. The embedded crack growth behaviour exhibited a significant level of agreement and accuracy, with observed that is a highly precise root mean square error (RMSE) value of 0.01 for an aspect ratio of 1.0. Meanwhile, the remaining values were 0.368 and 0.321 for 0.5 and 2.0 aspect ratios, respectively. Hence, the S-version FEM approach was thus highly successful in accurately determining the growth behaviour of embedded crack.

1. Introduction

Additive manufacturing (AM) is widely known for its reliance on the utilization of AlSi10Mg, an aluminum alloy highly favored in the industry. The preference for AlSi10Mg alloy is mainly driven by its remarkable mechanical properties, including excellent strength that enables it to withstand demanding applications. Additionally, the low density of AlSi10Mg makes it particularly well-suited for lightweight components, promoting efficient design and fuel economy. However, it is important to note that AlSi10Mg alloy, like any other material, is not impervious to failure. There are specific

* *Corresponding author.*
E-mail address: shamil@umpsa.edu.my

https://doi.org/10.37934/aram.130.1.3853

circumstances under which AlSi10Mg may experience limitations or mechanical shortcomings. One notable obstacle often encountered with this material is the occurrence of embedded cracks during the additive manufacturing process. One particular obstacle attached to this material is the appearance of embedded cracks that can arise during the process of printing.

Embedded cracks are cracks formed within the microstructure of the material that are not visible on the surface of the printed part. They can only be detected using non-destructive testing techniques such as X-ray or ultrasonic inspection. These cracks occur when the molten metal solidifies too quickly, resulting in internal stresses or the formation of pores that cause the material to crack. For instance, a microstructure with a high level of porosity can lead to internal stresses and cracks. Experimental results have shown that the fatigue capability of the material is extremely affected by several conditions such as crystallographic texture, defects, orientation distribution, and grain size [1–4]. Porosity negatively affects the mechanical properties of the final product, particularly its fatigue life performance. Therefore, embedded cracks act as stress concentrators, leading to a lower number of cycles before failure compared to parts without cracks. Defects provide a starting point for crack propagation, which can result in catastrophic failure. Embedded cracks significantly impact the fatigue life of a material, reducing its overall performance and potentially leading to failure.

To make sure that applications are safe to use, the eligibility of AM structural parts commonly requires a series of fatigue tests. However, conducting full-scale tests can be costly and time-consuming. Therefore, researchers have found that controlling parameters during the AM manufacturing process can improve fatigue resistance [5]. Numerous experimental works on the AlSi10Mg fatigue life have been conducted, considering factors such as build orientation, processing parameters, and post-processing techniques (e.g., heat treatment or surface treatment) [6–20]. In general, the fatigue resistance performance of AlSi10Mg parts is primarily influenced by residual pores, especially surface or subsurface faults, while strength and microstructural characteristics act as additional factors. Thus, two key approaches to enhance fatigue performance include reducing surface flaws through adjustments in the manufacturing setup and surface treatment, as well as strengthening the material through post-processing treatments. Pores and oxides (mostly alumina) function as initiation sites on the fracture surface and have been found to limit the fatigue performance in previous studies [19]. Romano *et al.,* have noted that manufacturing imperfections, particularly surface holes, regulate the fatigue strength of manufactured AlSi10Mg components [5,8]. Additionally, Romano *et al.,* demonstrated the utility of 3D CT scan works for detecting pores and the correlation between pore presence and fatigue resistance. Surface finishing and heat treatment (T6) have been shown to extend the fatigue lifetimes of AlSi10Mg products, especially at low stress levels, according to research by Aboulkhair *et al.,* [14]. Costas *et al.,* [21]conducted a numerical research and experiment on quasi-static loading of square boxes made of AlSi10Mg alloy produced through AM. The high porosity resulting from the process caused the material to fail in a quasi-brittle manner Read *et al.,* [22] utilized the energy density approach to analyse how process parameters influenced the development of porosity in AlSi10Mg alloy produced by AM. The results indicated that laser power, scan speed, and the interrelation between scan speed and scan spacing significantly impacted porosity development. The study also employed statistical analysis to determine reliable optimal process parameters.

Predicting the fatigue resistance of parts is crucial for achieving robust applications and designs in an industrial context. To address this challenge, finite element method (FEM) simulation software was utilized in this research to predict the behaviour of embedded cracks in AlSi10Mg alloy. These software simulations of cracks help save costs and time compared to conducting thousands of experimental tests. Among the simulation software options, the S-version Finite Element Method

(FEM) is particularly effective in predicting crack growth behaviour. The S-version FEM, introduced by Fish [23], stands out from commercial software due to its utilization of the mesh superimposed technique, where global-local meshes are overlay to target on local effects like holes or cracks. This technique reduces computational efforts, especially for large structures, as it eliminates the need for remeshing procedures necessary to model the development of crack configurations [24]. By employing the local mesh re-meshing procedure with an automatic meshing method, the creation of three-dimensional crack geometries becomes computationally systematic [25].

Given the limited scientific data to establish the credibility of AM materials, additional research is necessary to reinforce this manufacturing technology. A pivotal area of focus is fatigue crack analysis, essential for assessing structural integrity and reliability across engineering materials and preventing catastrophic failures resulting from crack propagation. Therefore, the objective of this study is to analyze the embedded crack growth by using S-version FEM as simulation software in AlSi10Mg alloy. Furthermore, the validation of S-version FEM output is carried out by configuration of experimental work to demonstrating the accuracy of software. The following section will brief the method of work.

2. Methodology

This section brief about the experimental and simulation setup used to investigate the embedded crack behaviour in AlSi10Mg alloy manufactured by AM process. This software built the model by creating a three-dimensional model by apply the material properties of AlSi10Mg alloy. The details of simulation setup are described including geometry, mechanical properties, and meshing methods. Then, the theory S-version Finite Element Method (FEM) is also explained, highlighting its reliability in predicting the material's response.

2.1 S-version FEM Formulation

The simulation software, S-version FEM, is a software that offers a better approach to analyze and investigate the embedded crack growth behaviour under a traction force is applied. By using the S-form FEM, an extensive report can be directed to comprehend the development and propagation of cracks within a structure subjected to different loads. This helps researchers and manufacturer to acquire valuable knowledge into the mechanics of crack growth and ultimately enhance the durability and reliability of materials and designs. The S-version FEM concept application is visually explained in Figure 1.

In S-version FEM, the meshing technique used is by applying the superimposing method into model. This technique employed the local mesh Ω^{L}, is set which set inside the global mesh area Ω^{G}. The crack is created as part of the local mesh and is overlaid onto the global mesh. The global mesh has a larger mesh size, while the local mesh has a finer mesh size. The simulation is then conducted on the local mesh, simplifying the model even for complex structures requiring crack analysis [25–27]. This approach reduces computation time without compromising accuracy.

The boundaries of each region are represented by Γ. Γ^{G} represents the boundary condition of the global element mesh, while Γ^{GL} represents the outer boundary condition of the local mesh. The displacement is denoted by Γ^{u} ,the force (traction) is denoted by Γ^{t} respectively.

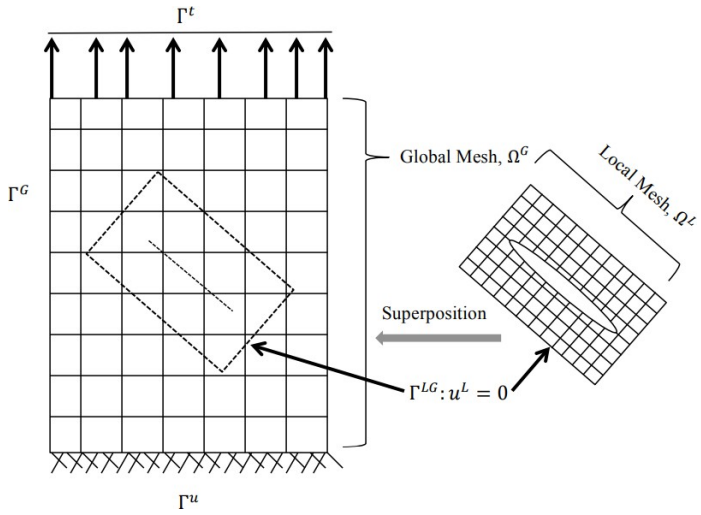

Fig. 1. S-version FEM concept application

The displacement equation, denoted by u, is applicable to both the global and local regions. u^G represents the displacement in the global area, while u^L represents the displacement in the local area. The displacement in the local area, u^L, is assumed be zero to ensure reliability at the boundary between the global and local regions. Eq. (1) provides the expression for the displacement function in both the global and local regions. For a detailed explanation of the input formulas for the displacement functions, refer to the study conducted by Shaari *et al.,* [28].

$$u_x = \begin{cases} \mathrm{u}_x^{\mathrm{G}} & \mathrm{x} \in \mathrm{G}^{\Omega} - \mathrm{G}^{\mathrm{L}} \\ u_x^G + u_x^L & \mathrm{x} \in \mathrm{G}^{\mathrm{L}} \end{cases} \tag{1}$$

In this study, Paris' law, a fundamental equation, is employed to predict the rate of fatigue fracture propagation, particularly in 2D and 3D problems. Eq. (2) represents the mathematical formulation of Paris' law used in this research.

$$\frac{da}{dN} = C\left(\Delta K_{eq}\right)^n \tag{2}$$

where

a	the crack depth,
N	the number of load cycles,
da/dN	denotes the crack growth rate,
ΔK_{eq}	the SIF range,
C and n	material constant of the specimen

2.2 Virtual Crack Closure Method

This subsection delves into the computation of fatigue crack growth. It involves calculating the energy release rate, G and stress intensity factor (SIF), which is assessed at the crack tip where higher stress levels indicate a greater propensity for crack advancement. The forthcoming discussion

outlines the method used to determine the SIF, K along the crack front. The SIF serves as a key parameter for predicting crack growth by assessing stress concentrations at the crack tip. The computation of SIF requires preliminary calculations using an established approach. The virtual crack closure method (VCCM) is a technique introduced by Rybicki and Kanninen in 1977 [29] for 2D analysis and later extended to 3D. This study adopts the VCCM technique as tailored by Okada *et al.,* [30] for skewed elements, making it suitable for semi-elliptical or non-symmetrical cracks. Figure 2 offers a simplified schematic of the VCCM, outlining the significance of upper and lower nodal forces, f, as well as displacement, u_i, is nodal displacement changes at different nodal number along the crack front.

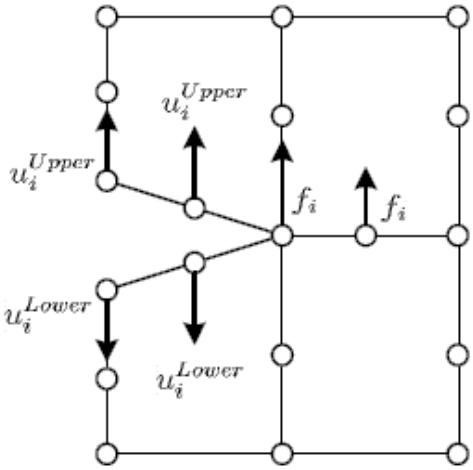

Fig. 2. Schematic illustration for calculation of nodal displacement

It is mentioned previously that the formulation in S-version FEM consists of both global and local element. However, for VCCM when the crack starts to propagate, the only changes is the relative displacement for local displacement since the crack is modelled at local region. Eq. (3) expresses the formulation for calculating the nodal displacements.

$$u_i = u^G + u^L$$

$$du_x = \left(u_G + u_L^{Upper}\right) - \left(u_G + u_L^{Lower}\right) = \left(u_L^{Upper} + u_L^{Lower}\right) \quad (3)$$

2.3 Material and Modeling

A 3D model of rectangular bar of AlSi10Mg alloy with intercept of embedded crack is modelled by S-version FEM. The dimension of rectangular bar was created by 50mm by 50mm and a height of 100mm as showed in Figure 3. The material characteristics of the as-built AlSi10Mg alloy, manufactured using Direct Metal Laser Sintering (DMLS), are provided in Table 1 [31]. The cross-sectional of the bar remains uniform throughout its length, making it a prismatic bar. The choice of a rectangular prismatic bar in this research enables the study of crack propagation in all directions, which is essential in the field of manufacturing where tension effects are significant. The lower surface of the bar is set as constraint in all directions with zero displacement, while the upper surface is subjected to a uniform load of 100MPa. This is to simulate the desired boundary conditions. The application of these boundary conditions on the global mesh is depicted in Figure 3.

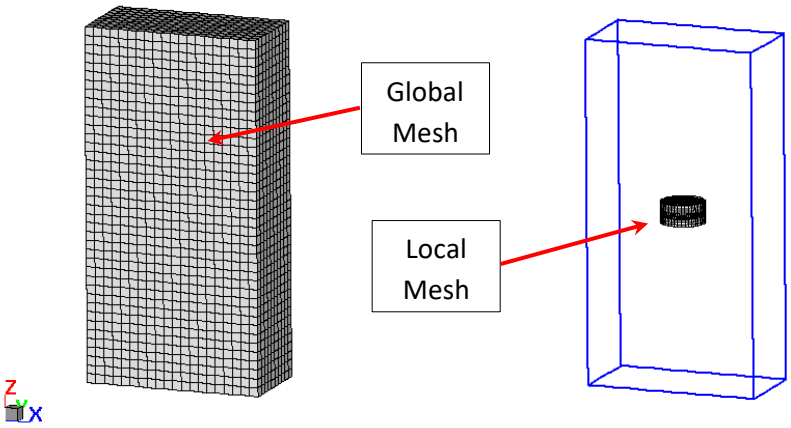

Fig. 3. S-version FEM (left) rectangular bar as global mesh (right) embedded crack as local mesh

Table 1
Geometry and material input parameter

Descriptions	Input
Type of alloy	AlSi10Mg
Young's Modulus, E	63.5 GPa
Paris Coefficient, C	1.85×10^{-9}
Fatigue Power Parameter, n	3.69
Width, w	50 mm
Thickness, t	50 mm
Height, h	100 mm
Load	100 MPa

Figure 4 illustrates a detailed sketch of the model, offering a clearer view of the crack's position and configuration. The initial crack is located at the midpoint of the rectangular bar and is oriented 90 degree to the loading axis. The 3D embedded crack is subsequently computed, and the results will be presented and discussed in the following sections. It is worth noting that for arbitrary or circular crack shapes, the position and angular direction of the embedded cracks begin and end at the same point.

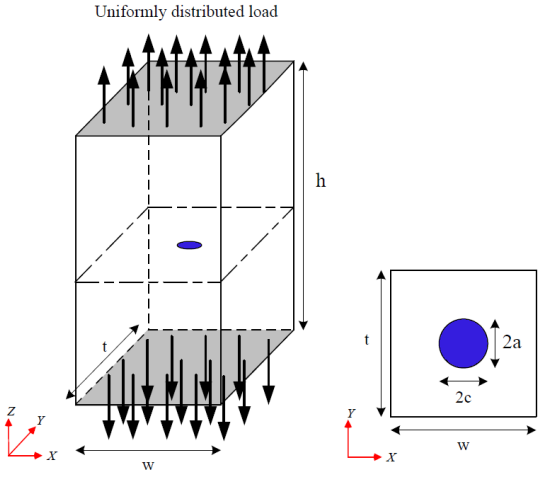

Fig. 4. Location of embedded crack and simulation condition

3. Results

This section presents the results of analysis on the microstructure and extensive investigation of crack propagation in AlSi10Mg alloy. The objective was to investigate the behaviour of embedded cracks by evaluating stress intensity factors (SIF). These results provide insights into the mechanical properties and behaviour of the material based on the computational method. In addition work for embedded crack growth is presented by different crack aspect ratios based on crack depth and length. Additionally, the effectiveness of the S-version Finite Element Method (FEM) in predicting crack propagation behaviour is validated, enhancing the reliability of the computational model used. The findings contribute to the understanding of AlSi10Mg alloy's microstructure and mechanical properties.

3.1 Microstructure of AlSi10Mg

The microstructural images of the AlSi10Mg alloy obtained from scanning electron microscopy (SEM) is presented in Figure 5 and Figure 6. Figure 5 displays the microstructure of the as-built AlSi10Mg specimen, while Figure 6 shows the microstructure after a heat treatment process involving annealing and solution heat treatment. The annealing process was carried out at 300°C for 2 hours, followed by solution heat treatment at 520°C for 6 hours.

In the SEM image of the as-built specimen, the silicon particles are evenly distributed within the aluminum matrix. Additionally, three distinct zones can be observed on the surface: coarse grains, fine grains, and the heat-affected zone. In the process of solidification, the core of the melt pool solidifies at the highest rate before gradually spreading towards the boundaries, where coarsening occurs. The overlapping of melt pools during the powder-bed laser-sintering process contributes to the formation of the heat-affected zone [32].

After the application of heat treatment, the silicon particles undergo spheroidization. This transformation occurs because of the solution heat treatment, which increases the popularize of silicon and leads to the formation of coarser particles. This process partially disrupts the eutectic Al-Si network structure [33,34]. It is worth noting that, following the spheroidization of silicon particles, an increase in porosity is observed in the AlSi10Mg alloy compared to as-built specimen. This can be clarified by the previously well-distributed silicon particles being covered by pores, while the coarsening of silicon particles occurs elsewhere in the material.

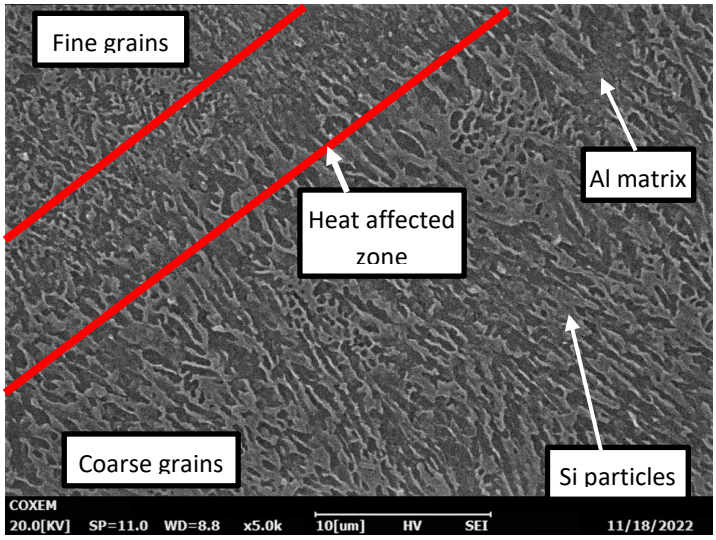

Fig. 5. SEM image of as-built AlSi10Mg alloy

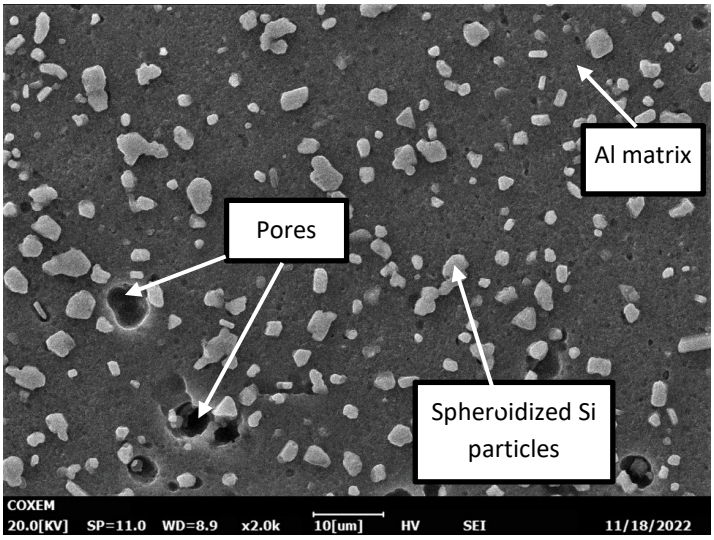

Fig. 6. SEM image of heat-treated AlSi10Mg alloy

3.2 Embedded Crack Propagation Analysis

In this research, a rectangular bar model consists of a three-dimensional embedded crack is simulated using S-version FEM. Figure 7 illustrates the propagation of the embedded crack, establishing a relationship between the crack depth, a, and the crack length, c. As the number of crack propagation steps increases, a circular shape peak propagation shape turns out to be more predominantly seen by the crack grows. The details are illustrated in Figure 8, which highlights both the crack's position and its angular orientation. The crack's initiation transpired within the internal structure of the model, after which it gradually extended outward along a trajectory depicted in the figure. The crack began propagated at 0 degree and finished at 360 degrees toward a path shown.

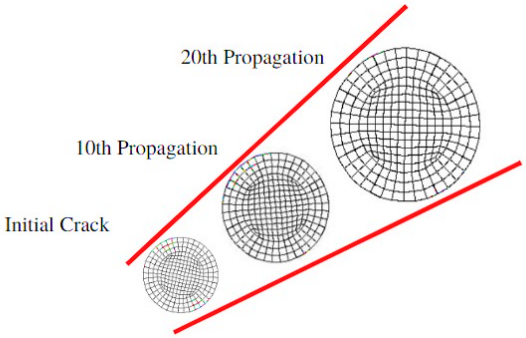

Fig. 7. Embedded crack propagation

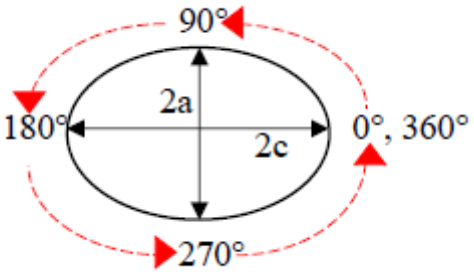

Fig. 8. Crack front angular direction

The simulation of embedded crack propagation is carried out up to 20 iterations. As shown in Figure 9, it depicts the development of beach marks from 0 to 15 steps. Throughout each phase of crack propagation, a consistent tensile load is applied. The crack depth and length are initially set at 2mm each. Then found the crack growth to approximately 8 mm and 9 mm for crack depth and length respectively at 15th step which showed as beach mark 8. As the cracks grow and approach a fully circular form, both the crack length and depth will have significantly increased. As the crack propagates through successive stages, approaching a fully circular crack form both the crack length and depth experience substantial growth.

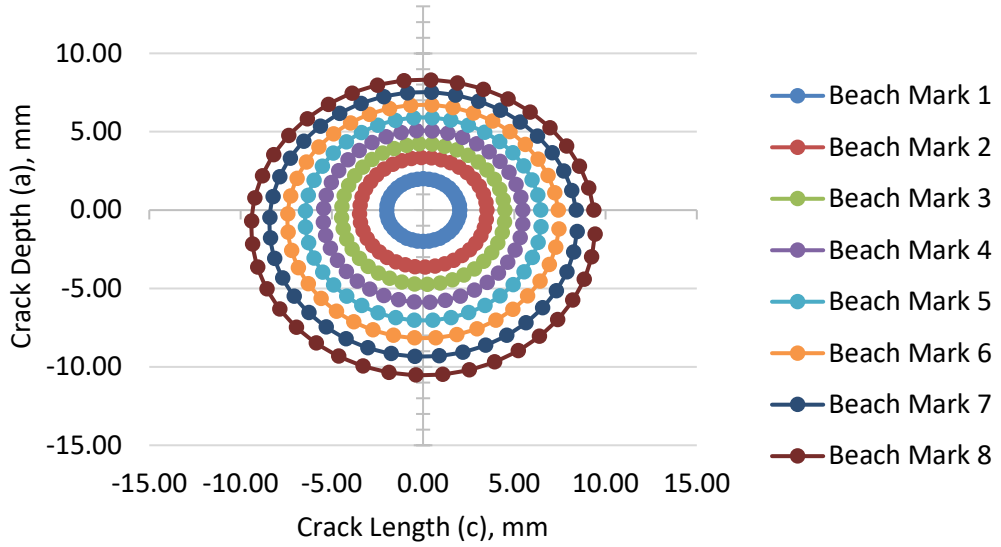

Fig. 9. Beach marks of embedded crack propagation

3.3 Stress Intensity Factor Analysis

Once the embedded crack propagates, the Stress Intensity Factor (SIF) provides insights into its likely propagation direction. Figure 10(a) illustrates the initial condition of the embedded crack based on the SIF. The horizontal axis represents the degree angle. From 0 to 90°, the SIF value is relatively low. However, it slightly increases as the angle approaches 360°. The SIF increased gradually from 0.15 MPa√m to 0.21 MPa√m at 360°. Meanwhile, a consistent trend of SIF value enables the embedded crack to uniformly propagate into a circular shape. Figure 10(b) demonstrates a steady SIF value of 4 MPa√m throughout the crack propagations at the 20th iteration. Further discussion and analysis of SIF at different initial cracks and aspect ratios will be presented in the subsequent section.

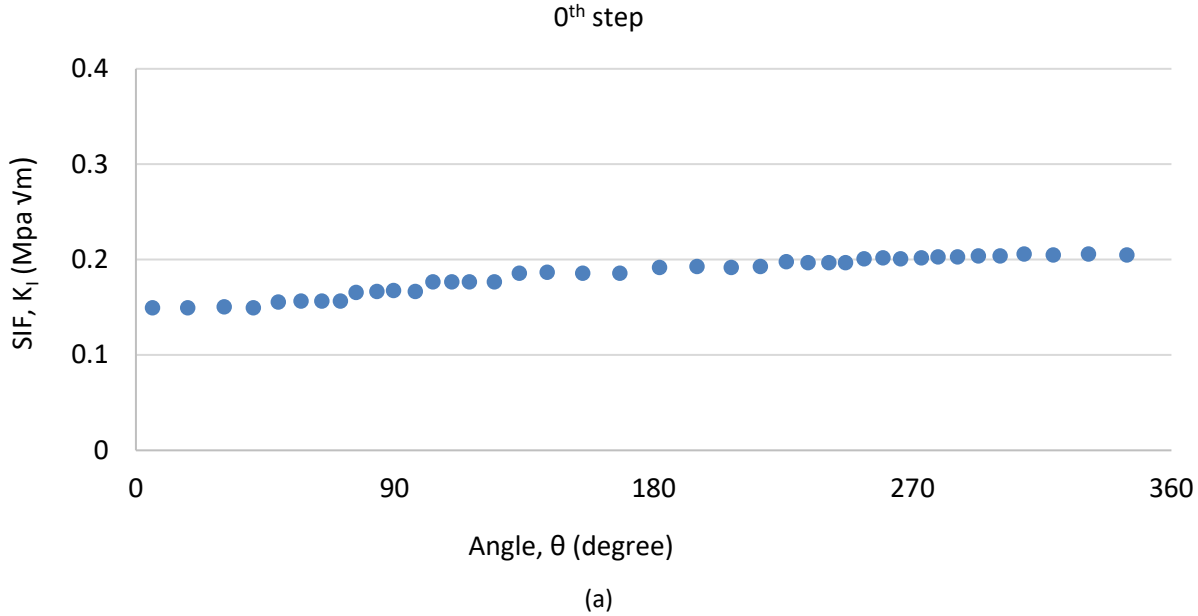

(a)

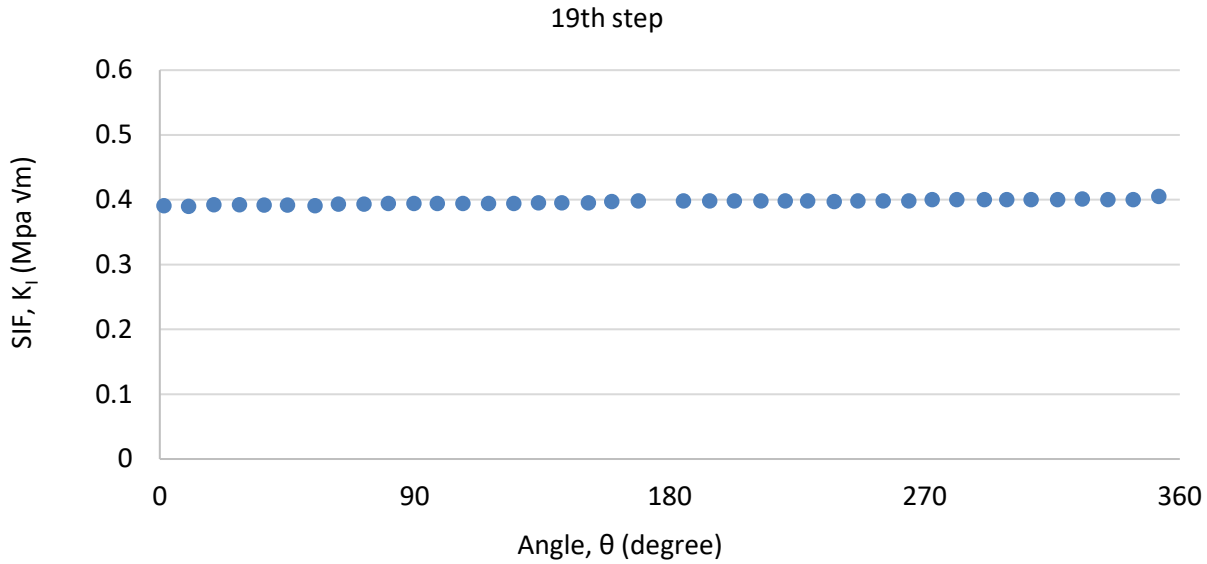

(b)

Fig. 10. Crack propagation in single embedded crack based on SIF at increment of (a) 0th step (b) 19th step

3.4 Evaluation of SIF for Different Aspect Ratio

In order to completely define the SIF of embedded crack, it is simulated again in SFEM to provide the SIF analysis for different initial crack sizes. Table 2 shows the different type of aspect ratios that are being studied in this research. With a stress ratio (R) of 0.1 and maximum stress σ_{max} of 100 MPa are applied, with crack depths of 2.0 mm and 4.0 mm chosen for each model. The three aspect ratios are applied to the same rectangular bar with identical boundary conditions, including a uniform tension loading on the top surface and fixed constraints at the other end, as depicted in Figure 4.

Consistent with the previous section, a steady and uniform SIF value indicates uniform crack propagation. Therefore, the subsequent studies focus on evaluating changes in SIF for aspect ratios ($a/c < 1$ or $a/c > 1$). Additionally, the objective is to investigate the aspect ratios that result in smoother cracks based on the SIF value. A larger surface area corresponds to a higher SIF value, and vice versa. The three different embedded crack configurations corresponding to their aspect ratios are simulated in the S-Version FEM. The shapes of the embedded cracks before reaching full propagation are shown in Figure 11(a) to (c). Under uniform tension loading, it is observed that the surface cracks converge to an aspect ratio of 1.0.

Table 2
Initial crack size for different aspect ratio

	Crack depth, a (mm)	Crack length, c (mm)	Aspect ratio, a/c
(a)	2.0	4.0	0.5
(b)	2.0	2.0	1.0
(c)	4.0	2.0	2.0

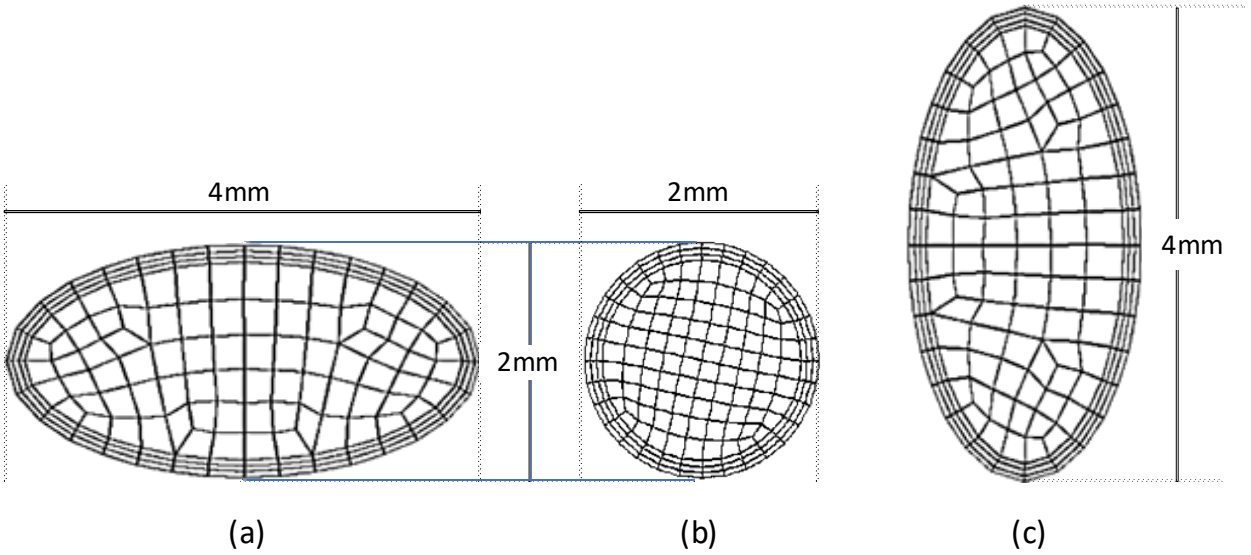

Fig. 11. Three selected initial crack shape

The changes in stress intensity factor, KI, for the three aspect ratios are evaluated and presented graphically in Figure 12, which combines the results of all the simulated embedded cracks. The graph reveals an inclination in the trend for aspect ratios of 0.5 and 2.0 between certain angles. At an aspect ratio of 0.5, the SIF spikes are observed at 0° and 180°. Similarly, for aspect ratio of 2.0, the SIF behaviour and trend are similar, with spikes occurring at 90° and 270° before declining again. This phenomenon arises because at these angles, the cracks experience the deepest point in their initial crack size. Cracks with deeper points propagate slower than the rest of the surface area, leading to smaller SIF values. Conversely, the SIF value increases more rapidly, and the crack propagates more rapidly in the inner surface area with a larger area. Thus, a larger and wider surface area facilitates crack propagation even more. This graph shows that at 0.5 and 2.0 aspect ratios as the trend can be seen inclining in between the angle. At aspect ratio of 0.5, the SIF trend can be seen spiking at 0 ° and 180 °. Notice that at aspect ratios of 2.0, the SIF behaviour and trend are similar. Hence, for aspect ratios of 2.0, the SIF also spiking at 90° and 270° before it declining again.

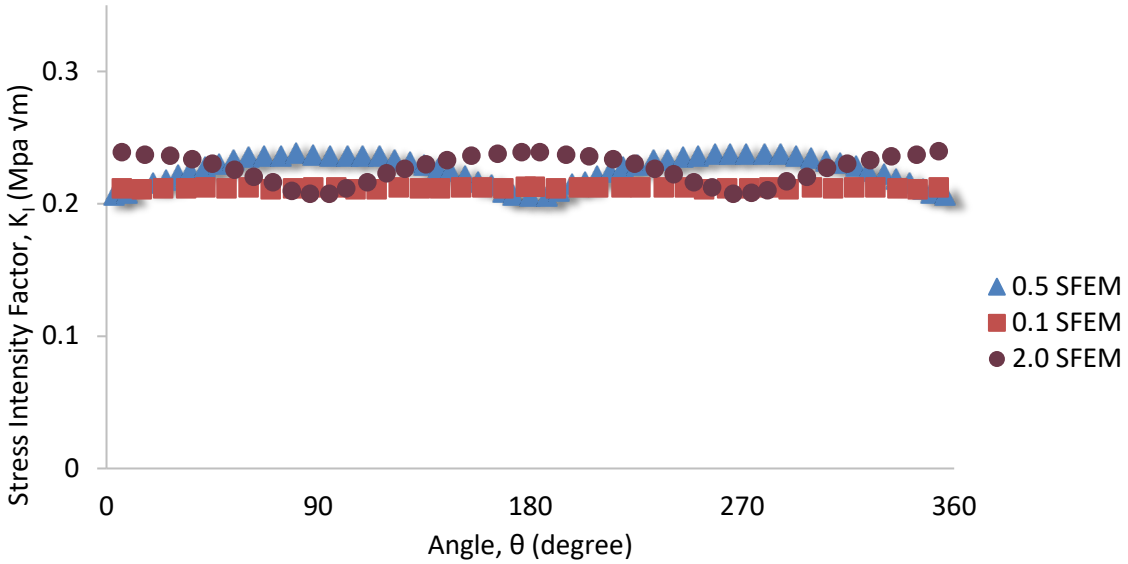

Fig. 12. SIF corresponding with different aspect ratio

3.5 Validation of S-version FEM

Three embedded cracks with different initial crack sizes are simulated in the S-Version FEM. The SIF values are calculated using the VCCM method, a numerical solution. A verification is conducted by comparing them with analytical solutions from Newman and Raju [35] for tension loading to ensure the accuracy of the SIF results obtained from the S-Version FEM.

The Eq. (4) is used to calculate the SIF value for tension loading of an embedded crack, where, S_t represents the tension load (100 MPa in this study), F is the boundary correction factor, and Q the shape factor, which varies based on different aspect ratios as shown in Eq. (5).

$$K_I = S_t \sqrt{\pi \frac{a}{Q}} F \tag{4}$$

$$Q = 1 + 1.464 \left(\frac{a}{c}\right)^{1.65} \qquad for \left(\frac{a}{c}\right) \leq 1$$

$$Q = 1 + 1.464 \left(\frac{c}{a}\right)^{1.65} \qquad for \left(\frac{a}{c}\right) > 1 \tag{5}$$

The SIF values obtained from the analytical solution and the S-Version FEM for each aspect ratio are then converted to normalized SIF using the formula $\frac{K_I}{S_t \sqrt{\pi \frac{a}{Q}}}$, as proposed by Newman and Raju in 1979 [35]. The normalized SIF values are plotted in Figure 13(a) to (c) to compare both sets of results. The graph demonstrates a close similarity between the S-Version FEM and analytical solutions.

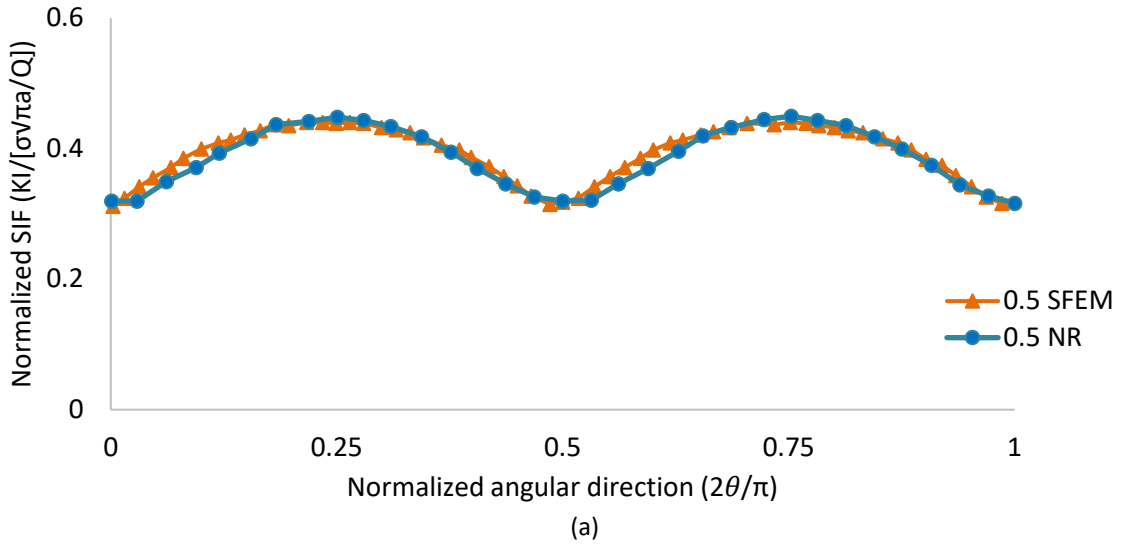

(a)

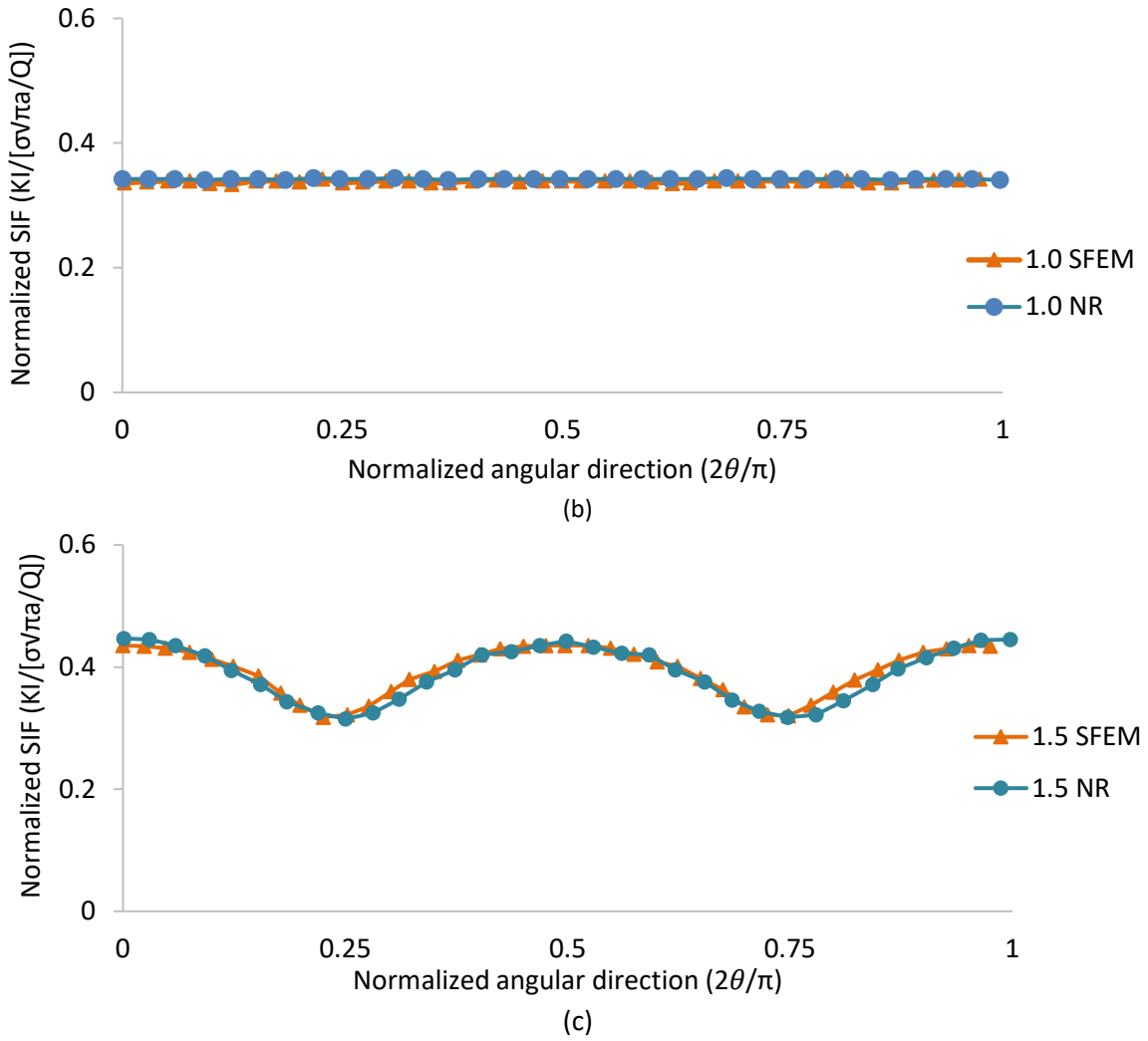

Fig. 13. Comparison of normalised SIF between S-Version FEM and Newman & Raju corresponding to different aspect ratio, (a) 0.5, (b) 1.0 and (c) 2.0

In order to evaluate the validation's reliability, the calculation of the root mean square error (RMSE) is carried out for each aspect ratio. The aspect ratio of 1.0 exhibits the lowest RMSE of 0.01, indicating higher accuracy in the validation. For aspect ratios of 0.5 and 2.0, the calculated errors are 0.368 and 0.321, respectively. These results indicate that the validations have a higher accuracy, with smaller RMSE values.

4. Conclusions

The prediction of embedded crack growth in AlSi10Mg AM material using the S-Version FEM has been successfully simulated. The key findings can be summarized as follows

i. Heat treatment processes affect the microstructure changes of the AlSi10Mg alloy, with defects formed due to rapid solidification during the printing process.
ii. The crack length and depth are directly proportional as the crack develops into a fully circular shape. Cracks with deeper points propagate slower than the rest of the surface area.
iii. The highest SIF value is recorded for an aspect ratio of 1.0. The influence of a larger and wider surface area on crack propagation is evident in the SIF values.

iv. The validation demonstrates good agreement between the S-Version FEM and analytical solutions for different initial crack sizes. The aspect ratio of 1.0 exhibits the highest accuracy, with the lowest RMSE of 0.01.

Acknowledgement
The author would like to acknowledge the Malaysian Ministry of Higher Education under the Fundamental Research Grant Scheme FRGS/1/2023/TK10/UMP/02/7 (university reference RDU230104) and Universiti Malaysia Pahang Al-Sultan Abdullah (RDU220367 and PGRS220386) for financial support. The authors would like to thank UMPSA for allowing the research to be conducted using high-performance computers (HPC).

References

[1] Castelluccio, Gustavo M., and David L. McDowell. "Mesoscale modeling of microstructurally small fatigue cracks in metallic polycrystals." *Materials Science and Engineering: A* 598 (2014): 34-55. https://doi.org/10.1016/j.msea.2014.01.015
[2] McDowell, David L. "Simulation-based strategies for microstructure-sensitive fatigue modeling." *Materials Science and Engineering: A* 468 (2007): 4-14. https://doi.org/10.1016/j.msea.2006.08.129
[3] Tang, Ming, and Petrus Christiaan Pistorius. "Fatigue Life Prediction for AlSi10Mg Components Produced by Selective Laser Melting." *International Journal of Fatigue* 125 (2019): 479–490. https://doi.org/10.1016/j.ijfatigue.2019.04.015
[4] Raja, A., Srinivasa Rakesh Cheethirala, Pallavi Gupta, Nilesh J. Vasa, and R. Jayaganthan. "A Review on the Fatigue Behaviour of AlSi10Mg Alloy Fabricated Using Laser Powder Bed Fusion Technique." *Journal of Materials Research and Technology* 17 (2022): 1013–1029. https://doi.org/10.1016/j.jmrt.2022.01.028
[5] Romano, S., A. Brückner-Foit, A. Brandão, J. Gumpinger, T. Ghidini, and S. Beretta. "Fatigue Properties of AlSi10Mg Obtained by Additive Manufacturing: Defect-Based Modelling and Prediction of Fatigue Strength." *Engineering Fracture Mechanics* 187 (2018): 165–189. https://doi.org/10.1016/j.engfracmech.2017.11.002
[6] Brandl, Erhard, Ulrike Heckenberger, Vitus Holzinger, and Damien Buchbinder. "Additive Manufactured AlSi10Mg Samples Using Selective Laser Melting (SLM): Microstructure, High Cycle Fatigue, and Fracture Behavior." *Materials & Design 34* (2012): 159–169. https://doi.org/10.1016/j.matdes.2011.07.067
[7] Siddique, hafaqat, Muhammad Imran, Miriam Rauer, Michael Kaloudis, Eric Wycisk, Claus Emmelmann, and Frank Walther. "Computed Tomography for Characterization of Fatigue Performance of Selective Laser Melted Parts." *Materials & Design* 83 (2015): 661–669. https://doi.org/10.1016/j.matdes.2015.06.063
[8] Mower, Todd M., and Michael J. Long. "Mechanical Behavior of Additive Manufactured, Powder-Bed Laser-Fused Materials." *Materials Science and Engineering: A* 651 (2016): 198–213. https://doi.org/10.1016/j.msea.2015.10.068
[9] Aboulkhair, Nesma T., Ian Maskery, Chris Tuck, Ian Ashcroft, and Nicola M. Everitt. "Improving the Fatigue Behaviour of a Selectively Laser Melted Aluminium Alloy: Influence of Heat Treatment and Surface Quality." *Materials & Design* 104 (2016): 174–182. https://doi.org/10.1016/j.matdes.2016.05.041
[10] Domfang Ngnekou, Julius N., Yves Nadot, Gilbert Henaff, Julien Nicolai, and Lionel Ridosz. "Influence of Defect Size on the Fatigue Resistance of AlSi10Mg Alloy Elaborated by Selective Laser Melting (SLM)." *Procedia Structural Integrity* 7 (2017): 75–83. https://doi.org/10.1016/j.prostr.2017.11.063
[11] Siddique, Shafaqat, Muhammad Imran, and Frank Walther. "Very High Cycle Fatigue and Fatigue Crack Propagation Behavior of Selective Laser Melted AlSi12 Alloy." *International Journal of Fatigue* 94 (2017): 246–254. https://doi.org/10.1016/j.ijfatigue.2016.06.003
[12] Brandão, Ana D., Johannes Gumpinger, Michael Gschweitl, Christoph Seyfert, Peter Hofbauer, and Tommaso Ghidini. "Fatigue Properties Of Additively Manufactured AlSi10Mg – Surface Treatment Effect." *Procedia Structural Integrity* 7 (2017): 58–66. https://doi.org/10.1016/j.prostr.2017.11.061
[13] Uzan, Naor Elad, Roni Shneck, Ori Yeheskel, and Nachum Frage. "Fatigue of AlSi10Mg Specimens Fabricated by Additive Manufacturing Selective Laser Melting (AM-SLM)." *Materials Science and Engineering: A* 704 (2017): 229–237. https://doi.org/10.1016/j.msea.2017.08.027
[14] Tang, Ming, and P. Chris Pistorius. "Oxides, Porosity and Fatigue Performance of AlSi10Mg Parts Produced by Selective Laser Melting." *International Journal of Fatigue* 94 (2017): 192–201. https://doi.org/10.1016/j.ijfatigue.2016.06.002

[15] Beretta, S., and S. Romano. "A Comparison of Fatigue Strength Sensitivity to Defects for Materials Manufactured by AM or Traditional Processes." *International Journal of Fatigue* 94 (2017): 178–191. https://doi.org/10.1016/j.ijfatigue.2016.06.020

[16] Romano, S., A. Brandão, J. Gumpinger, M. Gschweitl, and S. Beretta. "Qualification of AM Parts: Extreme Value Statistics Applied to Tomographic Measurements." *Materials & Design* 131 (2017): 32–48. https://doi.org/10.1016/j.matdes.2017.05.091

[17] Zhang, Changchun, Haihong Zhu, Hailong Liao, Yong Cheng, Zhiheng Hu, and Xiaoyan Zeng. "Effect of Heat Treatments on Fatigue Property of Selective Laser Melting AlSi10Mg." *International Journal of Fatigue* 116 (2018): 513–522. https://doi.org/10.1016/j.ijfatigue.2018.07.016

[18] Uzan, Naor Elad, Shlomo Ramati, Roni Shneck, Nachum Frage, and Ori Yeheskel. "On the Effect of Shot-Peening on Fatigue Resistance of AlSi10Mg Specimens Fabricated by Additive Manufacturing Using Selective Laser Melting (AM-SLM)." *Additive Manufacturing* 21 (2018): 458–464. https://doi.org/10.1016/j.addma.2018.03.030

[19] Romano, S., L. Patriarca, S. Foletti, and S. Beretta. "LCF Behaviour and a Comprehensive Life Prediction Model for AlSi10Mg Obtained by SLM." *International Journal of Fatigue* 117 (2018): 47–62. https://doi.org/10.1016/j.ijfatigue.2018.07.030

[20] Ngnekou, Julius Noel Domfang, Julien Nicolai, Yves Nadot, Gilbert Henaff, and Lionel Ridosz. "Influence of as-built surface and heat treatment on the fatigue resistance of Additively Layer Manufacturing (ALM) AlSi10Mg alloy." In *MATEC Web of Conferences*, vol. 165, p. 02004. EDP Sciences, 2018. https://doi.org/10.1051/matecconf/201816502004

[21] Costas, Miguel, David Morin, Mario de Lucio, and Magnus Langseth. "Testing and Simulation of Additively Manufactured AlSi10Mg Components under Quasi-Static Loading." *European Journal of Mechanics - A/Solids* 81 (2020): 103966. https://doi.org/10.1016/j.euromechsol.2020.103966

[22] Read, Noriko, Wei Wang, Khamis Essa, and Moataz M. Attallah. "Selective Laser Melting of AlSi10Mg Alloy: Process Optimisation and Mechanical Properties Development." *Materials and Design* 65 (2015): 417–424. https://doi.org/10.1016/j.matdes.2014.09.044

[23] Fish, J. "The S-Version of the Finite Element Method." *Computers & Structures* 43, no. 3 (1992): 539–547. https://doi.org/10.1016/0045-7949(92)90287-A

[24] Haziq Aiman, H. A., M. R.M. Akramin, M. N.M. Husnain, and M S Shaari. "Modelling of Crack Propagation for Embedded Crack Structure." In *Lecture Notes in Mechanical Engineering*, 11–19, 2020. https://doi.org/10.1007/978-981-15-4756-0_2

[25] Kikuchi, Masanori, Yoshitaka Wada, and Yulong Li. "Crack Growth Simulation in Heterogeneous Material by S-FEM and Comparison with Experiments." *Engineering Fracture Mechanics* 167 (2016): 239–247. https://doi.org/10.1016/j.engfracmech.2016.03.038

[26] Kikuchi, Masanori, Yoshitaka Wada, Yuto Shimizu, and Yulong Li. "Crack Growth Analysis in a Weld-Heat-Affected Zone Using S-Version FEM." *International Journal of Pressure Vessels and Piping* 90–91 (2012): 2–8. https://doi.org/10.1016/j.ijpvp.2011.10.001

[27] Akramin, M. R.M., A. K. Ariffin, Masanori Kikuchi, S. Abdullah, and N. Nik Abdullah. "Fatigue Crack Growth Analysis of Semielliptical Surface Crack." *Applied Mechanics and Materials* 471 (2014): 293–298. https://doi.org/10.4028/www.scientific.net/AMM.471.293

[28] Shaari, Mohd Shamil, Sylvia Urai, Akiyuki Takahashi, and Mohd Akramin Mohd Romlay. "Predicting Fatigue Crack Growth Behavior of Coalesced Cracks Using the Global-Local Superimposed Technique." *Frattura Ed Integrità Strutturale* 16, no. 62 (2022): 150–167. https://doi.org/10.3221/IGF-ESIS.62.11

[29] Rybicki, E. F., and M. F. Kanninen. "A Finite Element Calculation of Stress Intensity Factors by a Modified Crack Closure Integral." *Engineering Fracture Mechanics* 9, no. 4 (1977): 931–938. https://doi.org/10.1016/0013-7944(77)90013-3

[30] Okada, Hiroshi, Mayumi Higashi, Masanori Kikuchi, Yasuyoshi Fukui, and Noriyoshi Kumazawa. "Three Dimensional Virtual Crack Closure-Integral Method (VCCM) with Skewed and Non-Symmetric Mesh Arrangement at the Crack Front." *Engineering Fracture Mechanics* 72, no. 11 (2005): 1717–1737. https://doi.org/10.1016/j.engfracmech.2004.12.005

[31] Tan, S. P., M. A. Ramlan, M. S. Shaari, Akiyuki Takahashi, and M. R. M. Akramin. "Microstructural and Mechanical Characterization of AlSi10Mg Additively Manufactured Material Using Direct Metal Laser Sintering Technique." In *International Conference on Mechanical Engineering Research*, pp. 349-360. Singapore: Springer Nature Singapore, 2021. https://doi.org/10.1007/978-981-19-1457-7_28

[32] Thijs, Lore, Karolien Kempen, Jean Pierre Kruth, and Jan Van Humbeeck. "Fine-Structured Aluminium Products with Controllable Texture by Selective Laser Melting of Pre-Alloyed AlSi10Mg Powder." *Acta Materialia* 61, no. 5 (2013): 1809–1819. https://doi.org/10.1016/j.actamat.2012.11.052

[33] Zhuo, Longchao, Zeyu Wang, Hongjia Zhang, Enhuai Yin, Yanlin Wang, Tao Xu, and Chao Li. "Effect of Post-Process Heat Treatment on Microstructure and Properties of Selective Laser Melted AlSi10Mg Alloy." *Materials Letters* 234 (2019): 196–200. https://doi.org/10.1016/j.matlet.2018.09.109

[34] Alghamdi, F., X. Song, A. Hadadzadeh, B. Shalchi-Amirkhiz, M. Mohammadi, and M. Haghshenas. "Post Heat Treatment of Additive Manufactured AlSi10Mg: On Silicon Morphology, Texture and Small-Scale Properties." *Materials Science and Engineering A* 783 (2020). https://doi.org/10.1016/j.msea.2020.139296

[35] Raju, I.S., and J.C. Newman. "Stress-Intensity Factors for a Wide Range of Semi-Elliptical Surface Cracks in Finite-Thickness Plates." *Engineering Fracture Mechanics* 11, no. 4 (1979): 817–829. https://doi.org/10.1016/0013-7944(79)90139-5